AN IN-VITRO PRE-CLINICAL SAFETY COMPARISON OF MITRAGYNINE AND ITS OXIDATIVE METABOLITES: 7-HYDROXYMITRAGYNINE AND MITRAGYNINE PSEUDOINDOXYL

Authors: Patrick Kampmeyer, Benjamin Kampmeyer, Jacob Sinkwich, Kevin Weaver, Chandradeep Bollineni

ABSTRACT

Mitragyna speciosa, commonly known as Kratom, has become increasingly prevalent in the United States as a self-administered therapeutic agent for opioid withdrawal, anxiety relief, and chronic pain management. Mitragynine (MG), the principal alkaloid of M. speciosa, undergoes chemical transformation into 7-hydroxymitragynine (7HMG) via first-pass metabolism, and subsequently rearranges in plasma to form mitragynine pseudoindoxyl (MGP). Both metabolites exhibit substantially higher potency at opioid receptors compared to MG and contribute significantly to the analgesic effects of kratom, yet their safety has not yet been thoroughly investigated. This work is directed towards the assessment of the toxicological and pharmacological attributes of MG, 7HMG, and MGP. We found that 7HMG and MGP metabolites have lower cytotoxicity than MG in multiple cell lines. Furthermore, 7-HMG and MGP presented significantly less interaction with the known cardiotoxicity-associated target NAV1.5 when compared to MG. None of the three compounds presented significant activity at HERG or other cardiac voltage potential regulators. 7HMG and MGP selectively target the adrenergic receptor ADRA1A subtype as a partial antagonist whereas MG exhibits full antagonism at this subtype and additional partial antagonism at ADRA2A and ADRB2 which are not present for the metabolites. MG also demonstrated potent agonism at HTR1B and antagonism at HTR2R. None of the compounds produced measurable genotoxicity in COMET assays. In microsomal stability assays, 7HMG was found to be the most stable, followed by MG and then by MGP. We conclude that the metabolites 7HMG and MGP are unlikely to contribute additional toxicity beyond that associated with MG, as they

do not engage any novel off-targets and exhibit reduced activity at protein targets implicated in cardiotoxicity, hepatoxicity, and nephrotoxicity. Moreover, they do not exhibit greater cytotoxicity in human cells. Further in vivo studies are needed to validate these findings and confirm the relative safety profiles of these metabolites.

INTRODUCTION

Since the early 2000s, North America has faced an escalating public health crisis driven primarily by opioids, resulting in over a million overdose fatalities across the United States and Canada[1]. Initially fueled by the misuse of prescription opioids, the crisis has increasingly been dominated by highly potent illicit synthetic opioids, such as fentanyl and its analogues. Although effective medications for opioid use disorder (OUD) such as methadone and buprenorphine are available and proven to reduce mortality, their utilization is hindered by regulatory restrictions, logistical barriers, and social stigma, resulting in substantial gaps in treatment access and uptake[1]. In 2021 an estimated 2.5 million Americans had OUD, yet only about 22% received any MOUD[2]. Consequently, there remains significant unmet medical need for alternative therapeutic agents or adjuncts capable of reducing harm and assisting individuals in managing opioid dependence.

Kratom, an herbal supplement derived from the psychoactive Southeast Asian plant Mitragyna Speciosa, has gained attention in recent years due to its reported utility among individuals self-treating chronic pain, anxiety, depression, fatigue, and symptoms of opioid withdrawal[3]. Kratom is legally available in most of the United States, though not FDA approved. Its growth in popularity coincides with changes in opioid prescribing guidelines by the Center for Disease Control and Prevention in 2016 [2] and the rise in prevalence of fentanyl adulterated street opioids such as heroin which has spiked overdose[3]. Surveys indicate that many users specifically employ kratom to reduce or cease the use of prescription of illicit opioids, attributing sustained abstinence and symptom relief to kratom's effects[4].

The pharmacological effects of kratom are complex due to the presence of several structurally diverse alkaloids [4], each exhibiting distinct pharmacological profiles[5]. Kratom's effects are largely attributed to its most abundant alkaloid Mitragynine (MG), however, its first-pass metabolite 7-hydroxymitragynine (7HMG) has recently been elucidated as the primary mediator of its analgesic effects[5]. Further oxidative rearrangement of 7HMG in plasma yields Mitragynine Pseudoindoxyl (MGP)[6]. Both 7HMG and MGP have been characterized as G-biased mu-opioid receptor (MOR) and delt-opioid receptor (DOR) agonists, and this signaling bias is thought to be responsible for their reduced side effect profiles compared to classical opioids [7,8].

Despite the recognized significance of Kratom's oxidative metabolites 7HMG and MGP in mediating its analgesic effects, their individual toxicity and off-target interactions have yet to be investigated. In the present study, we aim to address this critical gap.

Materials and Methods

Reagents and Chemicals

Mitragynine (MG: 1) (purity ≥ 95%) was isolated and purified from a commercially available alkaloid-rich kratom extract. 7-Hydroxymitragynine (7HMG: 2) was semi-synthesized from mitragynine, and mitragynine pseudoindoxyl (MGP: 3) was semi-synthesized from 7HMG. The chemical structures and purity of 1-3 were confirmed by NMR and MS analysis. All solvents and reagents were of analytical grade. Key reagents, including (Bis(trifluoroacetoxy)iodo)benzene (PIFA), dichloromethane (DCM), methanol (MeOH), and anhydrous aluminum chloride, were obtained from Fisher Scientific.

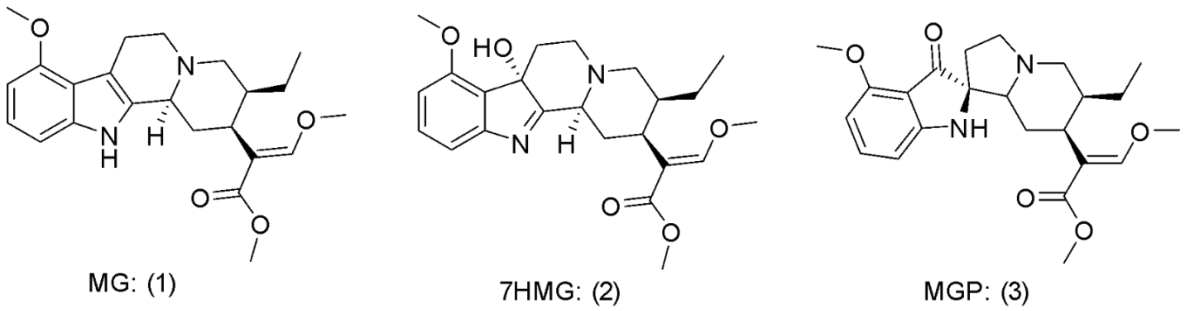

Fig. 1. Molecular Structure of Mitragynine, (MG); 7-hydroxymitragynine, (7HMG); Mitragynine Pseudoindoxyl, (MGP).

Chemistry

All chemicals were obtained from Sigma-Aldrich and used as received without further purification. Compound purification was carried out using a Büchi 815 Flash Chromatography System equipped with 230–400 mesh silica gel. Preparative high-performance liquid chromatography (Prep-HPLC) was performed on a Büchi 850 system using a C18 column under normal-phase conditions.

NMR spectra were acquired on a 400MHz Bruker Avance NEO with a 400MHz Avance NEO magnet and DCH CryoProbes. Data was processed using MestReNova software (version 10.0.2). Chemical shifts (δ) are reported in parts per million (ppm) relative to residual solvent peaks ($CDCl_3$: ^1H 7.26, ^{13}C 77.3; CD_3OD: ^1H 3.31, ^{13}C 49.0; DMSO-d_6: ^{13}C 39.5). Peak multiplicities are designated as follows: s (singlet), d (doublet), t (triplet), q (quartet), m (multiplet). Coupling constants (J) are provided in Hz.

Mass spectra were recorded using an Agilent 1100 LC MSD Model G1946D Mass Spectrometer with electrospray ionization (ESI). High-resolution mass spectra (HRMS) were obtained on a Waters Acquity Premier XE TOF LC-MS using ESI. Accurate masses are reported for the molecular ion $[M + H]^+$. Purity (≥95%) was confirmed by HPLC using a Waters 1525 Binary Pump, Waters 2489 UV-Vis detector, and a Waters XBridge C18 column (5 μm, 150 × 4.6 mm). The mobile phase consisted of solvent A (water with 0.1% trifluoroacetic acid) and solvent B (acetonitrile with 0.1% trifluoroacetic acid), with a gradient from 5% to 95% acetonitrile/water at a flow rate of 1 mL/min.

Extraction and Isolation of Mitragynine (1): Dried and powdered *Mitragyna speciosa* leaves (500 g) were extracted by refluxing with methanol (5 × 500 mL) for 40 min. The suspension was filtered after each extraction, and the solvent was evaporated under reduced pressure. The resulting residue was resuspended in 20% aqueous acetic acid (2 L) and extracted with petroleum ether (3 × 500 mL). The aqueous layer was cooled in an ice bath and basified to pH ~9 using 50% aqueous NaOH. The basified suspension was extracted with dichloromethane (DCM) (4 × 1 L). The combined organic layers were dried over anhydrous Na_2SO_4, filtered, and evaporated under reduced pressure. The crude extract was purified by flash column chromatography (gradient: 0–50% EtOAc in hexanes), yielding mitragynine (1) as the major component (3.5 g, 0.7% yield).

Characterization of Mitragynine (1):

IR (NaCl): 3363, 2950, 2796, 1698, 1643, 1570, 1508, 1435, 1310, 1275, 1255, 1148, 1106, 769, 734 cm^{-1}

^1H NMR (600 MHz, $CDCl_3$): δ 7.74 (s, 1H), 7.43 (s, 1H), 6.99 (t, J = 7.9 Hz, 1H), 6.90 (d, J = 8.0 Hz, 1H), 6.45 (d, J = 7.7 Hz, 1H), 3.87 (s, 3H), 3.72 (s, 3H), 3.71 (s, 3H), 3.18–3.08 (m, 2H), 3.06–2.99 (m, 2H), 3.00–2.93 (m, 1H), 2.94–2.90 (m, 1H), 2.57–2.42 (m, 3H), 1.83–1.75 (m, 2H), 1.62 (dt, J = 11.5, 3.2 Hz, 1H), 1.24–1.16 (m, 1H), 0.87 (t, J = 7.4 Hz, 3H).

^{13}C NMR (151 MHz, $CDCl_3$): δ 169.45, 160.75, 154.69, 137.41, 133.90, 121.98, 117.82, 111.67, 108.03, 104.37,

99.91, 61.74, 61.46, 57.94, 55.52, 53.98, 51.57, 40.87, 40.12, 30.14, 24.14, 19.28, 13.07.

HRMS (ESI): Calcd for $C_{23}H_{30}N_2O_4$ $[M + H]^+$: 399.2284; Found: 399.2285.

Preparation of 7-Hydroxymitragynine (2) from Mitragynine (1): Mitragynine (1, 2.00 g, 5.02 mmol) was dissolved in methanol (150 mL) with water (50 mL). The reaction mixture was cooled to 0 °C, and a solution of PIFA (2.16 g, 1.1 equiv) in methanol (22 mL) was added slowly over several minutes. The mixture was stirred at 0 °C for 1 h, then saturated aqueous $NaHCO_3$ was added. The mixture was extracted with dichloromethane, and the organic phase was evaporated under reduced pressure. Purification by silica gel column chromatography (gradient: 0–75% EtOAc in hexanes) yielded 7-hydroxymitragynine (2) as a light brown amorphous powder (640 mg, 32%).

Characterization of 7-Hydroxymitragynine (2):

IR (NaCl): 3436, 2952, 1702, 1645, 1599, 1487, 1461, 1436, 1270, 1246, 1145, 1078, 795, 738 cm^{-1}

^1H NMR (600 MHz, $CDCl_3$): δ 7.44 (s, 1H), 7.34 (t, J = 8.0 Hz, 1H), 7.24 (d, J = 7.6 Hz, 1H), 6.78 (d, J = 8.3 Hz, 1H), 3.91 (s, 3H), 3.80 (s, 3H), 3.70 (s, 3H), 3.31 (dd, J = 11.1, 2.6 Hz, 1H), 3.03 (ddt, J = 11.5, 5.5, 2.8 Hz, 2H), 2.84–2.75 (m, 3H), 2.67 (ddd, J = 12.3, 4.3, 2.6 Hz, 1H), 2.53–2.46 (m, 1H), 1.98–1.93 (m, 1H), 1.87 (ddd, J = 14.6, 12.2, 4.3 Hz, 1H), 1.70–1.54 (m, 3H), 1.26–1.23 (m, 1H), 0.81 (t, J = 7.3 Hz, 3H).

HRMS (ESI): Calcd for $C_{23}H_{30}N_2O_5$ $[M + H]^+$: 415.2233; Found: 415.2248.

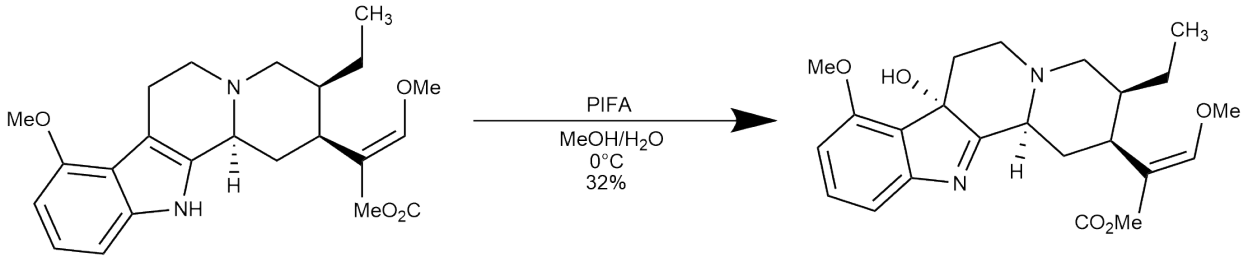

Fig. 2. Partial Synthesis of 7-hydroxymitragynine from Mitragynine.

Preparation of Mitragynine Pseudoindoxyl (3) from 7-Hydroxymitragynine (2): 7-Hydroxymitragynine (2, 200 mg, 0.48 mmol) was dissolved in dry DCM (6 mL), and $AlCl_3$ (350 mg, 2 equiv) was added. The reaction was stirred at room temperature (23 °C) for 2 h. The reaction was cooled and quenched with saturated aqueous $NaHCO_3$ (10 mL), then extracted with EtOAc (30 mL). The organic phase was washed with brine (20 mL), dried over anhydrous

Na_2SO_4, and evaporated under reduced pressure. Purification by silica gel chromatography (gradient: 1–5% MeOH in DCM) yielded mitragynine pseudoindoxyl (3) as a yellow amorphous powder (112 mg, 56%).

Characterization of Mitragynine Pseudoindoxyl (3):

IR (NaCl): 3350, 2947, 2794, 1687, 1615, 1502, 1343, 1269, 1246, 1148, 1079, 757 cm^{-1}

^{1}H NMR (600 MHz, $CDCl_3$): δ 7.32 (t, J = 8.1 Hz, 1H), 7.27 (s, 1H), 6.40 (d, J = 8.1 Hz, 1H), 6.13 (d, J = 8.1 Hz, 1H), 5.13 (s, 1H), 3.89 (s, 3H), 3.66 (s, 3H), 3.62 (s, 3H), 3.15–3.07 (m, 2H), 2.76 (dt, J = 11.9, 3.5 Hz, 1H), 2.38–2.29 (m, 2H), 2.29–2.18 (m, 1H), 2.14 (dt, J = 10.2, 6.3 Hz, 1H), 1.93–1.84 (m, 1H), 1.63 (dt, J = 11.3, 6.8 Hz, 1H), 1.49 (d, J = 11.3 Hz, 1H), 1.18 (ddd, J = 13.2, 7.8, 2.9 Hz, 1H), 1.11 (dd, J = 11.3, 3.6 Hz, 1H), 0.84 (t, J = 7.4 Hz, 3H).

^{13}C NMR (151 MHz, $CDCl_3$): δ 199.73, 169.05, 162.27, 160.40, 158.74, 138.85, 111.85, 109.96, 103.95, 99.21, 75.37, 73.38, 61.61, 55.86, 54.96, 53.35, 51.36, 40.28, 38.57, 35.25, 23.95, 19.47, 13.11.

HRMS (ESI): Calcd for $C_{23}H_{28}N_2O_5$ $[M + H]^+$: 415.2233; Found: 415.2216.

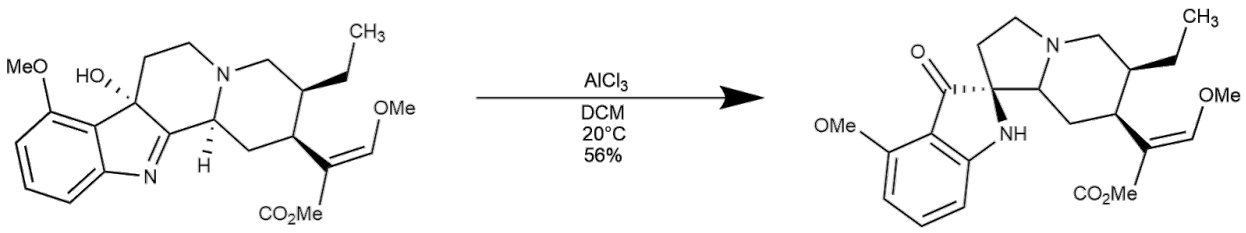

Fig. 3. Partial Synthesis of MGP from 7HMG

In Vitro Toxicology

Cell Culture

Two human cell lines were used for cytotoxicity assays: WI-38 and 293FT. WI-38 is a diploid human fibroblast cell line derived from fetal lung tissue (obtained from ATCC). 293FT is a human embryonic kidney cell line (Thermo Fisher Scientific). WI-38 cells were cultured in Dulbecco's Modified Eagle Medium (DMEM, high glucose) supplemented with 10% (v/v) heat-inactivated fetal bovine serum (FBS; Gibco) and 1% penicillin-streptomycin (100 U/mL penicillin, 100 µg/mL streptomycin). 293FT cells were maintained in the same DMEM + 10% FBS + 1% penicillin-streptomycin medium. Cultures were incubated at 37 °C in a humidified atmosphere of 5% CO_2. Cells were subcultured at ~80% confluency using 0.25% (w/v) trypsin-EDTA (Gibco).

In addition, human peripheral blood mononuclear cells (hPBMCs) were used as a primary cell model. Frozen Human PBMCs (obtained from ATCC) were suspended in a RPMI-1640 medium (Thermo Fisher Scientific) supplemented with 10% FBS and 1% penicillin-streptomycin and kept at 37 °C until use in cytotoxicity assays.

Cell Viability Assay

Cell viability was assessed using a WST-8 colorimetric assay (CCK-8 kit, Dojindo), in which a tetrazolium salt was added to a cell culture and subsequently reduced to formazan dye by cellular dehydrogenases in viable cells providing a direct measure of cell viability. WI-38 and 293FT cells were seeded in 96-well plates (Thermo Fisher Scientific) at densities of 8,000 WI-38 cells per well or 6,000 293FT cells per well and allowed to attach overnight. Cell cultures were then treated with serial dilutions of the test compounds: **1-3.** Triplicate wells were created for each active compound concentration with control wells containing vehicle without active compounds. After 96 hours of continuous exposure, the culture medium was removed from the wells. 10 µL of WST-8 reagent was then added to each well. Plates were then incubated at 37 °C for 4 hours. The absorbance in each well was measured at 450 nm with a reference wavelength at 650 nm using a microplate reader. Absorbance values, correlating with the number of metabolically active cells, in drug-treated wells were expressed as a percentage relative to absorbance in control wells. These data were used to calculate the IC50 for each cell line. IC_50 values were calculated by nonlinear regression, fitting the normalized dose-response data to a sigmoidal curve using GraphPad Prism (GraphPad Software).

Compound Profiling Assays

SAFETYscan E/IC50 ELECT profiling (Eurofins DiscoverX, San Diego, CA) was conducted to evaluate compound interactions across 78 human biological targets, including GPCRs, ion channels, nuclear hormone receptors, neurotransmitter transporters, kinases, and enzymes. Assays employed included PathHunter enzyme fragment complementation (EFC), FLIPR-based calcium flux and ion-channel assays, KINOMEscan kinase-binding assays, and enzymatic inhibition assays, conducted according to the manufacturer's standard protocols. Cells or purified enzyme preparations were incubated with compounds at increasing concentrations. GPCR activity was determined by monitoring intracellular cAMP levels and calcium mobilization using chemiluminescent and fluorescent detection methods, respectively. Ion channel blockade, including assays for hERG and NAV1.5, was evaluated through fluorescence-based thallium flux assays. Kinase-binding assays were performed using competitive

displacement from active-site ligands, quantified by qPCR. Enzymatic activity (e.g., COX1, COX2) was measured spectrophotometrically or fluorometrically based on substrate turnover. Data were analyzed with CBIS software (ChemInnovation, CA), calculating RC_{50} values via nonlinear regression analysis. Complete assay details and data processing procedures are provided in the supplementary information.

Aliquot concentrations and the escalating dosage range were selected based on the reported IC_{50} value of 7-hydroxymitragynine (7HMG) at the rat mu-opioid receptor (MOR), which is 53 nM as referenced in the ChEMBL database (ChEMBL ID: CHEMBL3751304). For validation, our in-house assay yielded a comparable RC_{50} of approximately 60 nM. The tested dosage range spanned from 0.51 nM to 3.3 µM using a 9-point, 3-fold serial dilution series. Compounds **1–3** were evaluated across this range to ensure adequate coverage of the expected activity window at the opioid receptor and to detect potential off-target interactions within physiologically relevant concentrations.

COMET Assay

Genotoxicity in human peripheral blood mononuclear cells (hPBMCs) was assessed for compounds 1-3 using COMET assays (ab238544, abcam). Cells were seeded on microplates and allowed to incubate overnight. Cells were then treated with one of three compounds, 1-3, at a concentration of 10uM and allowed to incubate for 24 hours. An additional set of wells were prepared as a control with DMSO without active compound. A positive control was prepared using 20uM of etoposide to ensure assay sensitivity. After incubation, the cells were removed from the wells by scraping with a rubber policemen. The cell suspension was transferred to a conical tube and centrifuged at 700 x g for 2 minutes. The cell pellets were washed using cold PBS containing no Mg^{2+} and Ca^{2+}, then again centrifuged at 700 x g for 2 minutes. The cells were then resuspended at 1 x 10^5 cells/mL in ice-cold PBS containing no Mg^{2+} and Ca^{2+}. The cell samples were combined with 0.75% low melting point agarose at a 1/10 ratio (v/v) and immediately transferred to a slide containing a base layer 1% normal melting point agarose. The slides were kept at 4°C for 15 minutes to solidify. The slides were then submerged in a lysis buffer containing 2.7M NaCl, 110mM EDTA, 10X lysis solution (abcam) at a 1/10 ratio (v/v), DMSO at a 1/10 ratio (v/v), and DI H_2O at 5/10 ratio (v/v). The slides remained in the lysis solution at 4°C for 60 minutes in the dark. The lysis buffer was aspirated and replaced with a pre-chill alkaline solution (0.3M NaOH, 1mM EDTA in DI H_2O) for 30 minutes at 4°C in the dark. The alkaline solution was then aspirated and replaced with an electrophoresis solution containing 90mM Tris Base,

89mM boric acid, and 2.5mM EDTA in DI H_2O at 4°C for 5 minutes. The slides were then immersed in fresh electrophoresis solution at 4°C for an additional 5 minutes. Slides were submerged in a cold TBE electrophoresis solution in an electrophoresis chamber where electrophoresis was carried out for 15 minutes at 35V and 300mA. Following electrophoresis, the slides were submerged for 2 minutes in a container containing pre chilled DI H_2O. This solution was aspirated and replaced twice more before a final immersion in cold 70% ethanol for 5 minutes. The slides were then removed from the ethanol solution and allowed to air dry. After drying, 100 uL of a diluted Vista Green DNA Dye was added to each well and allowed to incubate at room temperature for 15 minutes. The slides were then analyzed by epifluorescence microscopy using a FITC filter.

Microsomal Stability

Three separate sets of human liver microsome solutions containing 100µl of either MG, 7HMG or MGP in 10mM stock solution of DMSO in the presence of NADPH were placed in an incubator at 37C for a preincubation period of 15 minutes simulating the conditions of a human body. Samples of each set were taken from the incubator at their respective sample times of 0, 15, 30, 45, and 60 minutes. The absence of NADPH in figures "1,2,3" acts as the negative control for the assay. LCMS analysis was employed to quantify the percent compound remaining after incubation. Subsequently, the half-life (T1/2) is estimated from the slope of the initial linear range of the logarithmic curve of compound remaining (%) versus time, assuming first order kinetics given by the following formula:

Molecular Docking

Protein Preparation

A structural model of the human Nav1.5 (SCN5A) voltage-gated sodium channel was prepared based on the cryo-EM structure of Nav1.5 in complex with quinidine (PDB ID: 6LQA), which provides high-resolution detail of the pore domain and ligand binding site. The protein was preprocessed for docking by removing all non-receptor components, including quinidine as the co-crystallyzed ligand, solvent molecules, and additional subunits.

Hydrogen atoms were added in accordance with physiological pH (7.4), and partial atomic charges were assigned using the Gasteiger method. Local energy minimization was performed to optimize side-chain conformations and relieve steric clashes. The resulting structure was exported in PDBQT format to enable flexible-ligand docking using AutoDock-based methods.

Ligand Preparation

The structures of MG**,** 7HMG**,** MGP, and quinidine were imported in SMILES format, and converted into PDB format using MMFF94 force field to obtain a low-energy geometry. OpenBabel was used to assignGasteiger partial charges and define atom types compatible with AutoDock**.**

Docking Method

The co-crystallized quinidine ligand was used to define the center of the docking grid. A box size of 10 Å per dimension was specified to encompass the pore domain of the NaV1.5 channel. A 5 Å interaction cutoff was applied to identify ligand–receptor contacts within the binding site. During ligand preparation, all non-ring single bonds were designated as rotatable, except those within amide linkages, which were kept rigid to preserve their planar geometry. Docking was performed using AutoDock Vina, and the top 10 binding poses were retained for each ligand.

RESULTS AND DISCUSSION

Cytotoxicity and Cell Viability

The cytotoxic effects of compounds **1–3** were evaluated in three human cell models including WI-38 lung fibroblasts, 293FT kidney cells, and primary hPBMCs. IC_{50} values were determined using a 4-day WST-8 assay (Table 1). Mitragynine (MG) exhibited the highest cytotoxicity overall, particularly in WI-38 and 293FT cells. In hPBMCs, mitragynine pseudoindoxyl (MGP) showed the lowest IC_{50} (3.2 μM), though the difference was not significantly different from MG (5.70 μM). We found that MG demonstrated moderate to high cytotoxicity in kidney-derived 293FT cells which is consistent with prior rodent studies in which high doses of mitragynine caused renal tubular degeneration, glomerular congestion, and interstitial inflammation (Harizal et al., 2010). Although clinical data are limited, several case reports and poison center records describe acute kidney injury in kratom users (Sangani et al. 2021). While no direct evidence currently links mitragynine to cyclooxygenase (COX)-mediated renal injury, our data show that MG is a moderate inhibitor of both COX-1 and COX-2. These enzymes are constitutively expressed in various renal structures where they regulate renal blood flow, glomerular filtration rate, and fluid balance. It is also well established that COX-2 inhibition by NSAIDs is a primary mechanism of acute

kidney injury (Bindu et al. 2020). Therefore, our findings suggest that oxidative metabolism of MG to 7HMG and MGP may attenuate renal toxicity, as both metabolites displayed lower cytotoxicity in kidney cells.

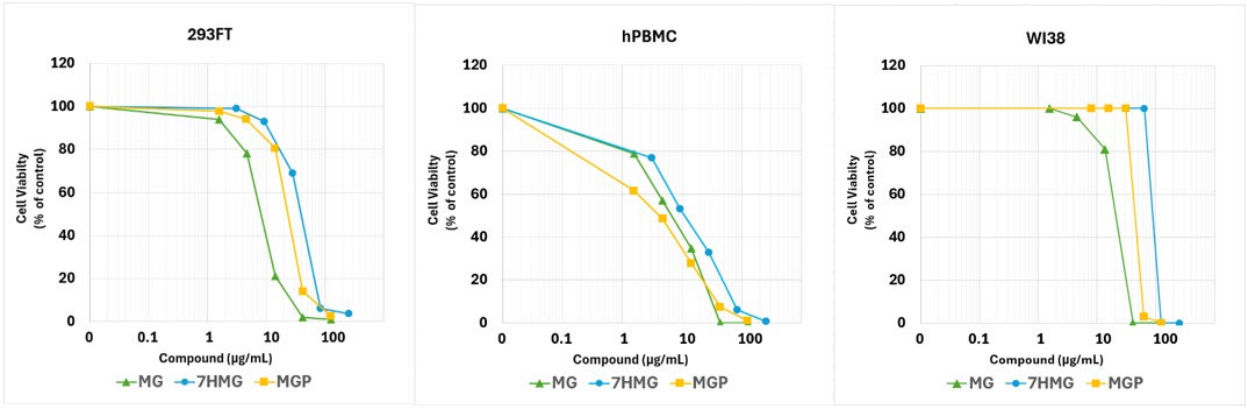

Fig. 4. Dose-dependent cytotoxicity of MG, 7HMG, and MGP in human cell lines. Cell viability was assessed in 293FT kidney cells (left), primary hPMBCs (middle), and WI-38 lung fibroblasts (right) following 4-day treatment with increasing concentrations of each compound using the WST-8 assay. MG showed the highest cytotoxicity in 293FT and WI-38 cells. In hPBMCs, MGP exhibited the lowest IC50, though viability trends were similar between compounds. Data reflect means from representative experiments with viability expressed as a percentage of untreated control.

Genotoxicity

Human peripheral blood mononuclear cells (hPBMCs) were treated with 1-3 at a concentration of 10umg/mL for 24 hours. A positive control group was treated with etoposide at 20uM for 4 hours. Following treatment, cells were collected and subjected toa Comet assay to assess DNA damage. Under these conditions, none of the test compounds induced detectable DNA damage.

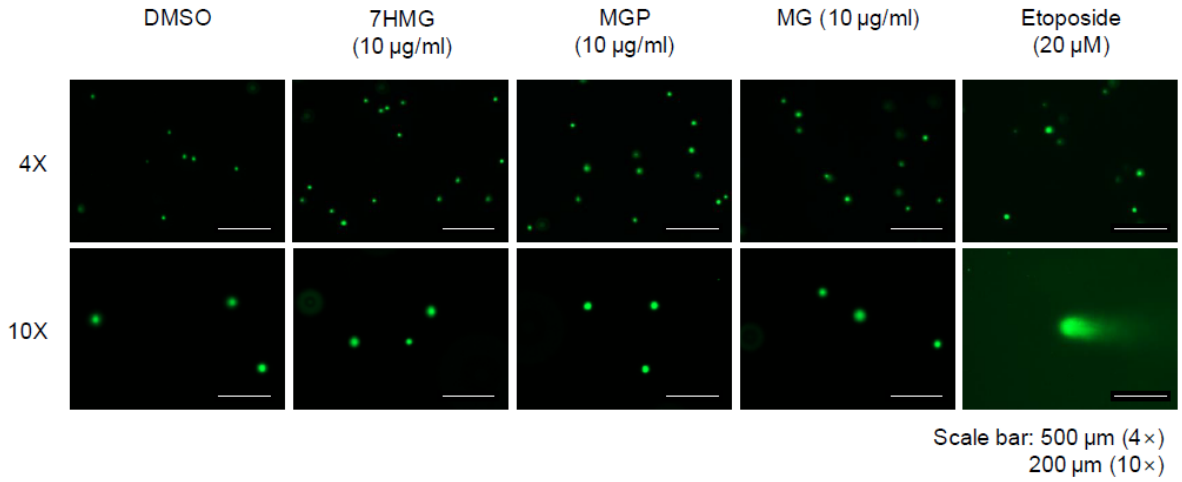

Fig. 4: Comet assay of hPMBCs treated with test compounds 1-3 (10µg/mL, 24 h) or etoposide (20µM, 4h). Cells were assessed for DNA damage using alkaline conditions. No significant DNA damage was observed in cells treated with compounds 1-3, whereas etoposide (positive control) produced market comet trails indicative of genotoxicity.

Off-Target Screening

The pharmacological profiling of **1-3** was performed across a comprehensive panel of 78 assays, identifying significant receptor and enzyme interactions relevant to their therapeutic and safety profiles. Assay results were considered insignificant if the max response was less than 50% of the control and the EC50 was greater than 10uM.

Adrenergic Activity

Functional assays revealed that MG had little ADRA1A agonist activity but acted as a full antagonist with an IC50 of 0.46uM and a max response of 99.45% inhibition at 10uM. 7HMG and MP also had little ADRA1A agonist activity with max responses of 6.9% and 17.96% inhibition respectively at 10uM. 7HMG and MP exhibited stronger ADR1A antagonist activity with IC50s of 6.56uM and 4.49uM and max responses of 65.4% and 80.1% at 10uM respectively. MG and MP had little ADRA2A and ADRB2 agonist activity but demonstrated stronger antagonist activity at these subtypes. MG acted as a strong ADRA2A antagonist with an IC50 of 8.2uM and a max response of 58.82% inhibition at 10uM. MG also acted as a strong antagonist at the ADRB2 subtype with an IC50 of 5.16uM and a max response of 70.46% at 10uM. MP elicited a partial inhibitory response at ADRA2A and ADRB2 with max responses of 18.37% inhibition and 29.78% inhibition at 10uM respectively. 7HMG exhibited little agonist and antagonist activity at both ADRA2A and ADRB2 receptors. These data suggest that while MG displays broad, moderate efficacy across adrenergic targets, 7HMG and MP are more selective toward a single subtype.

Table 1: Adrenergic activity of MG, 7HMG, and MGP. Agonist and Antagonist activity was studied with RC50 and Maximum response reported.

Compound	Target	Activity Type	RC50 (uM)	Max Response (%)
MG	ADRA1A	Agonist	10	0.64
		Antagonist	**0.46**	**99.45**
7HMG	ADRA1A	Agonist	10	6.9
		Antagonist	**6.56**	**65.36**
MGP	ADRA1A	Agonist	10	17.96
		Antagonist	**4.49**	**80.08**
MG	ADRA2A	Agonist	10	1.74
		Antagonist	**8.2**	**58.82**
7HMG	ADRA2A	Agonist	10	4.67
		Antagonist	10	7.1
MGP	ADRA2A	Agonist	10	5.63
		Antagonist	10	18.37
MG	ADRB2	Agonist	10	0
		Antagonist	**5.16**	**70.46**
7HMG	ADRB2	Agonist	10	0.3
		Antagonist	10	2.1
MGP	ADRB2	Agonist	10	0
		Antagonist	10	29.78

Opioidergic Activity

MG and its metabolites 7HMG, and MGP have previously been characterized as partial agonists or antagonists at opioid receptors, with a growing body of evidence highlighting their atypical G-protein biased signaling profiles [7,9–11]. MGP and 7HMG have been reported as partial agonists at the human mu-opioid receptor (hMOR) and competitive antagonists at the kappa and delta opioid receptors (hMOR, hDOR), while MG is reported to be a partial agonist at MOR and weak antagonist at both DOR and KOR[9].

Our findings are mostly consistent with earlier reports although we reveal a few previously unreported or conflicting features. MG showed negligible agonist activity at all three human opioid receptor subtypes. Prior studies have a reported modest efficacy (~65% Emax)[7] which suggests MG's functional activity may be assay specific. KOR has not previously been reported for 7HMG, though we observe it to have significant partial antagonistic activity. Prior studies which had used rodent derived KOR preparations reported negligible KOR activity for MGP, whereas we found both MGP and 7HMG to have moderate efficacy (~45% Emax) at human KOR, with 7HMG effective at lower concentrations than MGP . Our results also indicate that 7HMG and MGP work as full agonists rather than antagonists at DOR.

Table 2: Opioidergic activity of MG, 7HMG, and MGP. Agonist and Antagonist activity was studied with RC50 and Maximum response reported.

Compound	Target	Activity Type	RC50 (uM)	Max Response (%)
MG	OPRD1	**Agonist**	**2.84**	**68.46**
		Antagonist	10	6.79
7HMG	OPRD1	**Agonist**	**0.07**	**90.21**
		Antagonist	10	0
MGP	OPRD1	**Agonist**	**0**	**94.26**
		Antagonist	10	0
MG	OPRK1	Agonist	10	8.2
		Antagonist	10	9.05
7HMG	OPRK1	**Agonist**	**1.78**	**58.4**
		Antagonist	10	13.67
MGP	OPRK1	Agonist	10	14.69
		Antagonist	**7.85**	**57.91**

MG	OPRM1	Agonist	10	41.8
		Antagonist	10	35.1
7HMG	OPRM1	**Agonist**	**0.06**	**83.96**
		Antagonist	10	0
MGP	OPRM1	**Agonist**	**0**	**85.66**
		Antagonist	10	0

Cyclooxegynase Activity

Cycloxygenase enzymes, COX-1 and COX-2 are known to mediate the inflammatory response via prostaglandin biosynthesis from arachidonic acid (AA)[8]. COX-1, constitutively expressed in various tissues, maintains physiological functions such as gastric mucosal protection and platelet aggregation, whereas COX-2 is typically inducible, upregulated at inflammatory sites by cytokines and other stimuli[8]. COX-2-derived prostaglandins promote hallmark symptoms of inflammation, including vasodilation, edema, and pain, making both enzymes primary targets for anti-inflammatory therapy. Nonsteroidal anti-inflammatory drugs (NSAIDs) target these enzymes and thereby reduce prostaglandin production and inflammatory responses.

Despite their efficacy, NSAIDs are associated with well-characterized adverse effects linked to COX inhibition. Nonselective NSAIDs cause gastrointestinal toxicity due to suppression of protective COX-1-derived prostaglandins, whereas selective COX-2 inhibitors (coxibs), despite reducing gastrointestinal complications, carry cardiovascular risks arising from disrupted prostacyclin-thromboxane balance, leading to increased incidence of thrombotic events[10].

Given that Kratom's pharmacological profile may partially involve modulation of COX pathways, this mechanism could be implicated in its known renal toxicity. The involvement of COX-1/COX-2 pathways in the antinociceptive effects of Kratom has been confirmed only recently [12]. Preclinical studies indicate MG inhibits dose-dependent hepatic and renal toxicity, with significant histopathological changes observed at higher concentrations (100 mg/kg), symptoms which mimic those associated with prolonged NSAID use[13]. Although rare, there have been a few clinical case reports which have documented Kratom induced acute liver injury [14], and less commonly, kidney injury [15].

Table 3: Cyclooxygenase activity of MG, 7HMG, and MGP.

Compound	Target	Activity Type	RC50 (uM)	Max Response (%)
MG	COX1	**Inhibitor**	**2.45**	**108.51**
7HMG	COX1	**Inhibitor**	**9.15**	**54.36**
MGP	COX1	**Inhibitor**	**4**	**84.55**
MG	COX2	**Inhibitor**	**1.47**	**154.74**
7HMG	COX2	**Inhibitor**	**4.24**	**94.99**
MGP	COX2	**Inhibitor**	**10**	**149.55**

Serotonergic Activity

Several alkaloids from Kratom, including MG, have shown interactions with 5-HT1 and 5-HT2 subfamilies [3], which may be partially responsible for the reported mood-enhancing and stimulant effects [1,2]. Furthermore, MG has been shown to have micromolar affinity at 5-HT2B receptor and to induce the head twitch response (HTR) in rodents in a dose-dependent manner as a result [4]. Binding studies at 5-HT1A have shown differential activities of the minor Kratom alkaloids paynantheinine and speciogynine with MG [5], where all three display either full or partial agonistic activity. However, far less is know about MGs activity at 5-HT1B and 5-HT2B receptor subtypes, which are associated with antidepressant activity and cardiovascular safety respectively [6,7]. We found MG produced profound responses at both 5-HT1B and 5-HT2B receptors while 7HMG and MP exhibited minimal to no activity.

Table 4: Serotonergic activity of MG, 7HMG, and MGP.

Compound	Target	Activity Type	RC50 (uM)	Max Response (%)
MG	HTR1B	**Agonist**	**1.09**	**110.79**
		Antagonist	10	0
7HMG	HTR1B	Agonist	10	12.53
		Antagonist	10	0
MGP	HTR1B	Agonist	10	6.78
		Antagonist	10	0
MG	HTR2B	Agonist	10	0
		Antagonist	**1.34**	**90.64**
7HMG	HTR2B	Agonist	10	0

MGP	HTR2B	Antagonist	10	26.54
		Agonist	10	0
		Antagonist	10	45.2

Sodium Channel Activity:

Cardiotoxicity is the leading cause of drug attrition during preclinical development, clinical trials, and post marketing surveillance representing approximately 40% of all drug withdrawals due to safety concerns[16]. Specifically, prolongation of the QT interval represented 33% of drug withdrawals during the same period. While not life threatening in itself, QT prolongation can lead to lethal arrhythmias such as ventricular tachycardia and torsades de pointes. Dysfunction of either Nav1.5 or hERG channels has been linked to prolonged QT intervals.

NAV1.5 is a voltage-gated sodium channel found in several tissue types but is predominantly expressed in cardiac muscle cells. It is responsible for initiating the cardiac action potential by mediating sodium influx into the cytosol, resulting in depolarization of the cell. NAV1.5 is the primary target of Class I antiarrhythmic drugs which inhibit its activity. Undesired or excessive inhibition of NAV1.5 can lead to QT interval prolongation increasing the risk of arrhythmias.

Table 5: NAV1.5 activity of MG, 7HMG, and MGP.

Compound	Target	Activity Type	RC50 (uM)	Max Response (%)
MG	NAV1.5	**Blocker**	**9.39**	**51.85**
7HMG	NAV1.5	Blocker	10	22.6
MGP	NAV1.5	Blocker	10	39.13

Non-linear regression and dose response analysis yielded an IC50 for MG of 9.39 μM. The IC50 of 7HMG and MGP were not conclusively determined but were found to be >10 μM. The max inhibition of MG, 7HMG and MGP were 51.85%, 22.6% and 39.13% respectively. Lidocaine Hydrochloride, a sodium channel blocker, was used as a

reference control. Lidocaine indicated an IC50 of 15.58 μM. These data indicate all 3 compounds exhibit partial inhibition of the NAV1.5 channel with MG exhibiting the greatest amount of inhibition. Based on these data, we can conclude that MG has a greater inhibitory effect on NAV1.5 when compared to 7HMG and MGP.

Microsomal Stability

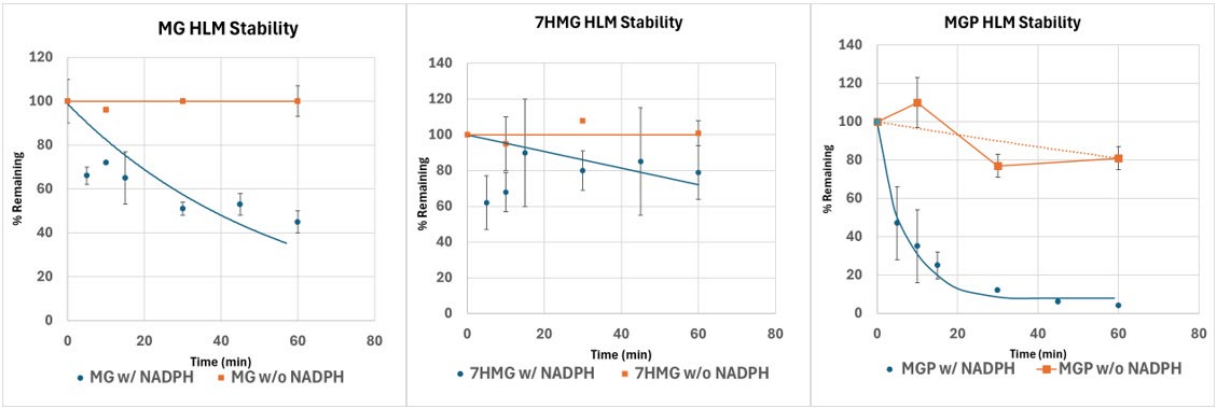

Figure 1: Microsomal stability of mitragynine (MG), 7-hydroxymitragynine (7HMG), and mitragynine pseudoindoxyl (MGP) in the presence and absence of NADPH. Human liver microsomes (HLMs) were incubated with each compound at 37 °C, and samples were collected over 60 minutes to assess percent compound remaining by LC-MS. Reactions were conducted with (+NADPH) or without (–NADPH) the cofactor to evaluate NADPH-dependent metabolism. MG (left) and MGP (right) showed rapid metabolic degradation in the presence of NADPH, indicating high intrinsic clearance. In contrast, 7HMG (middle) exhibited relatively greater stability over time, suggesting lower metabolic turnover and potentially higher bioavailability. These data support the hypothesis that 7HMG is a more metabolically stable metabolite and may contribute to prolonged systemic activity.

Sodium Channel Activity

Cardiotoxicity is the leading cause of drug attrition during preclinical development, clinical trials, and post marketing surveillance representing approximately 40% of all drug withdrawals due to safety concerns.

NAV1.5 is a voltage-gated sodium channel found in several tissue types but is predominantly expressed in cardiac muscle cells. It is responsible for initiating the cardiac action potential by mediating sodium influx into the cytosol, resulting in depolarization of the cell. NAV1.5 is the primary target of Class I antiarrhythmic drugs which inhibit its activity. Undesired or excessive inhibition of NAV1.5 can lead to QT interval prolongation increasing the risk of arrhythmias.

Compound	Target	Activity Type	RC50 (uM)	Max Response (%)
MG	NAV1.5	**Blocker**	**9.39**	**51.85**
7HMG	NAV1.5	Blocker	10	22.6
MGP	NAV1.5	Blocker	10	39.13

Non linear regression and dose response analysis yielded an IC50 for MG of 9.39 uM. The IC50 of 7HMG and MP were not conclusively determined but were found to be >10uM. The max inhibition of MG, 7HMG and MP were 51.85%, 22.6% and 39.13% respectively. Lidocaine Hydrochloride, a sodium channel blocker, was used as a reference control. Lidocaine indicated an IC50 of 15.58 uM. These data indicate all 3 compounds exhibit partial inhibition of the NAV1.5 channel with MG exhibiting the greatest amount of inhibition. Based on these data, we can conclude that MG has a greater inhibitory effect on NAV1.5 when compared to 7HMG and MP.

In-Silico Investigation

NAV1.5 Channel Inhibition

Despite its potential therapeutic value, kratom use has been linked to many occurrences of multiorgan toxicity and cardiotoxicity[1,2]. Acute cardiac effects include tachycardia and hypertension[3]. Prior in-vitro studies have indicated

that long-term kratom use can lead to prolonged QT syndrome [4] and it is thought that hERG1a/1b channel function and trafficking may explain such observations[4]. These effects may be exacerbated by co-administration of kratom with other substances, potentially due to MG's inhibition of the CYP2D6 enzyme which affects drug metabolism[5].

To our knowledge, no detailed investigations have examined the interaction between MG and the cardiac sodium channel Nav1.5 which is responsible for initiation of the cardiac cycle. Pharmacological inhibition of Nav1.5 is known to cause acquired long QT syndrome, potentially resulting in cardiac arrhythmias[6].

To investigate the interaction between MG and the cardiac sodium channel Nav1.5, we conducted computational docking studies using AutoDock Vina and a crystallized structure of Nav1.5 (PDB 6LQA). The antiarrhythmic drug quinidine was co-crystallized within the Nav1.5 binding pocket and served as a reference ligand to guide initial docking simulations. MG was also overlaid with quinidine and additional known Nav1.5 channel blockers to identify pharmacophoric elements crucial for channel interaction.

Quinidine binds beneath the selectivity filter in the pore domain of Nav1.5, interacting with residues from channel repeats I, III, and IV, thereby tightening the intracellular gate and preventing sodium ion permeation[7]. We suspect that MG may have a similar mode of action.

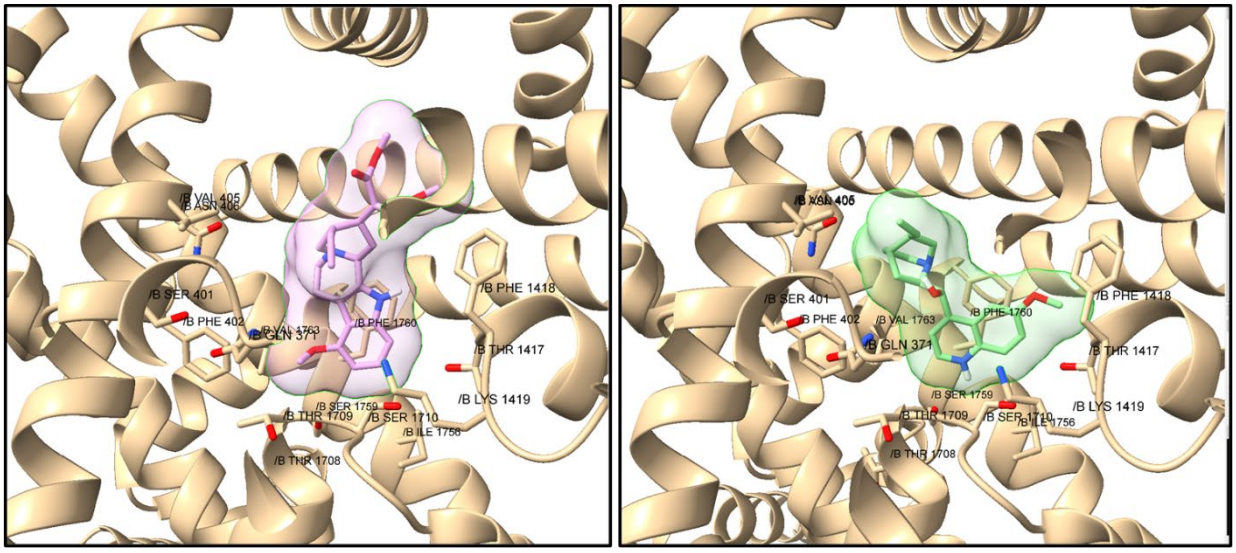

Figure 2 : Computational docking of MG, 7HMG, and MGP to the cardiac sodium channel Nav1.5 reveals potential interactions linked to cardiotoxicity. To evaluate the potential role of kratom alkaloids in cardiotoxicity, in silico docking studies were performed using AutoDock Vina and the human Nav1.5 crystal structure (PDB: 6LQA), with quinidine as a reference ligand. All tested compounds demonstrated conserved π–π stacking interactions with

residues GLN^371 and VAL^405 near the central pore region of the channel. Quinidine showed the most extensive binding profile, forming additional interactions with PHE^1760, ASN^406, LEU^409, SER^1759, and THR^1417, consistent with its known ability to inhibit Nav1.5 and induce QT prolongation. MG bound less extensively but maintained key interactions via its indole core, while polar substitutions on 7HMG and MP appeared to reduce π–π stacking with PHE^1760, potentially diminishing their binding affinity. These findings suggest that MG may share structural determinants with known Nav1.5 inhibitors, raising the possibility of a mechanistic link between kratom alkaloids and adverse cardiac electrophysiology.

All ligands demonstrated conserved pi-pi stacking with GLN^{371} and VAL^{405} residues located near the central pore region of the channel, although quinidine demonstrated a more complex interaction profile compared to MG, 7HMG, and MP.

All ligands exhibited conserved π–π stacking interactions with GLN^{371} and VAL^{405}, residues situated near the central pore region of the channel. However, quinidine displayed a more extensive interaction profile compared to mitragynine (MG), 7-hydroxymitragynine (7HMG), and mitragynine pseudoindoxyl (MGP), engaging additional residues through both π–π and hydrogen bonding interactions.

GLN^{371}, THR^{1417}, and SER^{1759} are positioned to form hydrogen bonds with polar functional groups of quinidine. In the case of MG, π–π stacking interactions are observed with GLN^{371}, VAL^{405}, and PHE^{1760} via the indole core. However, π–π stacking with PHE^{1760} is likely attenuated in 7HMG and MP, where polar substitutions (e.g., hydroxyl or carbonyl groups) at the C3 position of the indole ring may disrupt the planarity and electron density of the aromatic system necessary for effective stacking.

compd	**Residue Interaction**
Quinidine	$GLN^{371}, PHE^{1760}, VAL^{405}, ASN^{406}, LEU^{409}, PHE^{402}, SER^{1759}, THR^{1417}$
MG	$GLN^{371}, VAL^{405}, THR^{1417}, PHE^{1760}$
7HMG	$GLN^{371}, VAL^{405}, THR^{1417}$
MGP	$GLN^{371}, VAL^{405}, THR^{1417}$

Inhibition of COX1 and COX2

Cycloxygenase enzymes, COX-1 and COX-2 are known to mediate the inflammatory response via prostaglandin biosynthesis from arachidonic acid (AA)[8]. COX-1, constitutively expressed in various tissues, maintains physiological functions such as gastric mucosal protection and platelet aggregation, whereas COX-2 is typically inducible, upregulated at inflammatory sites by cytokines and other stimuli[8]. COX-2-derived prostaglandins promote hallmark symptoms of inflammation, including vasodilation, edema, and pain, making both enzymes primary targets for anti-inflammatory therapy. Nonsteroidal anti-inflammatory drugs (NSAIDs) target these enzymes and thereby reduce prostaglandin production and inflammatory responses. However, the involvement of the COX-1/COX-2 pathways in the pharmacological effects of kratom remains poorly understood and has only recently been explored[9].

Despite their efficacy, NSAIDs are associated with well-characterized adverse effects linked to COX inhibition. Nonselective NSAIDs cause gastrointestinal toxicity due to suppression of protective COX-1-derived prostaglandins, whereas selective COX-2 inhibitors (coxibs), despite reducing gastrointestinal complications, carry cardiovascular risks arising from disrupted prostacyclin-thromboxane balance, leading to increased incidence of thrombotic events[10].

Given that kratom's pharmacological profile may partially involve modulation of COX pathways, understanding its safety and potential organ toxicity becomes crucial. Preclinical studies indicate mitragynine exhibits dose-dependent hepatic and renal toxicity, with significant histopathological changes observed at higher concentrations (100 mg/kg), raising concerns similar to those associated with prolonged NSAID use[2]. Although rare, there have been a few clinical case reports have documented Kratom induced acute liver injury[11] and less commonly, kidney injury [12].

Conclusions

To our knowledge, this study represents the first in-vitro preclinical evaluation of mitragynine's (MG) oxidative metabolites, 7-hydroxymitragynine (7HMG) and mitragynine pseudoindoxyl (MGP). Our findings regarding the activity of MG, 7HMG, and MGP at the mu-opioid receptor (MOR) and delta opioid receptor (DOR) are consistent with other reports. We also identified previously unreported agonistic activity of 7HMG and MGP at the kappa-opioid receptor (KOR).

Prior serotonergic activity at the 1A subtype has previously been reported. We found additional strong agonistic effects at HTR1B and antagonism at HTR2B. 7HMG and MGP had significantly more bias toward the HTR2B subtype. All three compounds engaged the adrenergic receptor ADR1A as antagonists, with MG exhibiting the greatest potency. MG also demonstrated complete inhibition of both COX-1 and COX-2 while 7HMG and MGP fully inhibited COX-2 and had reduced inhibition of COX-1.

Our results also highlight a potential cardiotoxic mechanism specific to MG via inhibition of the cardiac sodium channel NAV1.5. This effect was observed to a much lesser extent with 7HMG and MGP. Docking simulations suggest that MG may inhibit NAV1.5 by pi-pi stacking interactions similar to those observed with the antiarrhythmic drug quinidine. Substitution at the C3 position of the indole ring in 7HMG and MGP may disrupt these interactions which could explain their reduced inhibition.

All three compounds exhibited mild inhibition of the hERG potassium channel at concentrations up to 10 μM, with 7HMG showing the lowest maximal effect (E_max = 15%). Previous studies have reported upregulation of hERG1a–Hsp90 complexation, which may influence channel trafficking and function. In this study, we also identified Nav1.5 inhibition as an additional potential mechanism contributing to cardiotoxicity. Future investigations should assess the relative contributions of these pathways to QT interval prolongation and overall cardiac risk associated with kratom alkaloids.

Genotoxicity assessment using the Comet assay in human peripheral blood mononuclear cells (hPBMCs) revealed no significant DNA damage for MG, 7HMG, or MGP. Additional assays such as the micronucleus test and Ames

test may be necessary to evaluate other forms of genomic stress. Long term rodent studies might also help to fully exclude carcinogenic risk.

Microsomal stability assays demonstrated that MGP was rapidly metabolized, indicating poor hepatic stability relative to MG and 7HG. Of the three, 7HMG exhibited the greatest metabolic stability. These findings suggest that despite MGP's pharmacological potency, its systemic exposure is likely limited due to rapid hepatic clearance.

To summarize, our findings suggest that oxidative metabolites 7HMG and MGP are unlikely to contribute additional toxicity beyond that observed for MG. Both metabolites exhibit reduced engagement of off-targets associated with cardiac, hepatic, and renal toxicity, and comparable or lower toxicity in human cell models. Further in vivo studies are needed to understand the extent to which these effects impact normal physiological function.

References

(1) Fischer, B.; Robinson, T. 'Safer Drug Supply' Measures in Canada to Reduce the Drug Overdose Fatality Toll: Clarifying Concepts, Practices and Evidence within a Public Health Intervention Framework. *J. Stud. Alcohol Drugs* **2023**, jsad.23-00195. https://doi.org/10.15288/jsad.23-00195.

(2) Jones, C. M.; Han, B.; Baldwin, G. T.; Einstein, E. B.; Compton, W. M. Use of Medication for Opioid Use Disorder Among Adults With Past-Year Opioid Use Disorder in the US, 2021. *JAMA Netw Open* **2023**, *6* (8), e2327488. https://doi.org/10.1001/jamanetworkopen.2023.27488.

(3) Garcia-Romeu, A.; Cox, D. J.; Smith, K. E.; Dunn, K. E.; Griffiths, R. R. Kratom (Mitragyna Speciosa): User Demographics, Use Patterns, and Implications for the Opioid Epidemic. *Drug and Alcohol Dependence* **2020**, *208*, 107849. https://doi.org/10.1016/j.drugalcdep.2020.107849.

(4) Flores-Bocanegra, L.; Raja, H. A.; Graf, T. N.; Augustinović, M.; Wallace, E. D.; Hematian, S.; Kellogg, J. J.; Todd, D. A.; Cech, N. B.; Oberlies, N. H. The Chemistry of Kratom [*Mitragyna Speciosa*]: Updated Characterization Data and Methods to Elucidate Indole and Oxindole Alkaloids. *J. Nat. Prod.* **2020**, *83* (7), 2165–2177. https://doi.org/10.1021/acs.jnatprod.0c00257.

(5) Obeng, S.; Kamble, S. H.; Reeves, M. E.; Restrepo, L. F.; Patel, A.; Behnke, M.; Chear, N. J.-Y.; Ramanathan, S.; Sharma, A.; León, F.; Hiranita, T.; Avery, B. A.; McMahon, L. R.; McCurdy, C. R. Investigation of the Adrenergic and Opioid Binding Affinities, Metabolic Stability, Plasma Protein Binding Properties, and Functional Effects of Selected Indole-Based Kratom Alkaloids. *J. Med. Chem.* **2020**, *63* (1), 433–439. https://doi.org/10.1021/acs.jmedchem.9b01465.

(6) Kruegel, A. C.; Uprety, R.; Grinnell, S. G.; Langreck, C.; Pekarskaya, E. A.; Le Rouzic, V.; Ansonoff, M.; Gassaway, M. M.; Pintar, J. E.; Pasternak, G. W.; Javitch, J. A.; Majumdar, S.; Sames, D. 7-Hydroxymitragynine Is an Active Metabolite of Mitragynine and a Key Mediator of Its Analgesic Effects. *ACS Cent. Sci.* **2019**, *5* (6), 992–1001. https://doi.org/10.1021/acscentsci.9b00141.

(7) Kamble, S. H.; León, F.; King, T. I.; Berthold, E. C.; Lopera-Londoño, C.; Siva Rama Raju, K.; Hampson, A. J.; Sharma, A.; Avery, B. A.; McMahon, L. R.; McCurdy, C. R. Metabolism of a Kratom Alkaloid Metabolite in Human Plasma Increases Its Opioid Potency and Efficacy. *ACS Pharmacol. Transl. Sci.* **2020**, *3* (6), 1063–1068. https://doi.org/10.1021/acsptsci.0c00075.

(8) Váradi, A.; Marrone, G. F.; Palmer, T. C.; Narayan, A.; Szabó, M. R.; Le Rouzic, V.; Grinnell, S. G.; Subrath, J. J.; Warner, E.; Kalra, S.; Hunkele, A.; Pagirsky, J.; Eans, S. O.; Medina, J. M.; Xu, J.; Pan, Y.-X.; Borics, A.; Pasternak, G. W.; McLaughlin, J. P.; Majumdar, S. Mitragynine/Corynantheidine Pseudoindoxyls As Opioid Analgesics with Mu Agonism and Delta Antagonism, Which Do Not Recruit β-Arrestin-2. *J. Med. Chem.* **2016**, *59* (18), 8381–8397. https://doi.org/10.1021/acs.jmedchem.6b00748.

(9) Wilson, L. L.; Chakraborty, S.; Eans, S. O.; Cirino, T. J.; Stacy, H. M.; Simons, C. A.; Uprety, R.; Majumdar, S.; McLaughlin, J. P. Kratom Alkaloids, Natural and Semi-Synthetic, Show Less Physical Dependence and Ameliorate Opioid Withdrawal. *Cell Mol Neurobiol* **2021**, *41* (5), 1131–1143. https://doi.org/10.1007/s10571-020-01034-7.

(10) Annuar, N. A. K.; Azlan, U. K.; Mediani, A.; Tong, X.; Han, R.; Al-Olayan, E.; Baharum, S. N.; Bunawan, H.; Sarian, M. N.; Hamezah, H. S.; Jantan, I. An Insight Review on the Neuropharmacological Effects, Mechanisms of Action, Pharmacokinetics and Toxicity of Mitragynine. *Biomedicine & Pharmacotherapy* **2024**, *171*, 116134. https://doi.org/10.1016/j.biopha.2024.116134.

(11) Masae, M.; Cheaha, D. Effect of Long-Term of Kratom-Aqueous Extract Containing Addictive Dose of Mitragynine on Liver and Kidney in Mice. *Conference Proceedings* **2023**.

(12) Post, S.; Spiller, H. A.; Chounthirath, T.; Smith, G. A. Kratom Exposures Reported to United States Poison Control Centers: 2011–2017. *Clinical Toxicology* **2019**, *57* (10), 847–854. https://doi.org/10.1080/15563650.2019.1569236.

(13) Lu, J.; Wei, H.; Wu, J.; Jamil, M. F. A.; Tan, M. L.; Adenan, M. I.; Wong, P.; Shim, W. Evaluation of the Cardiotoxicity of Mitragynine and Its Analogues Using Human Induced Pluripotent Stem Cell-Derived Cardiomyocytes. *PLoS ONE* **2014**, *9* (12), e115648. https://doi.org/10.1371/journal.pone.0115648.

(14) Kong, W. M.; Chik, Z.; Ramachandra, M.; Subramaniam, U.; Aziddin, R. E. R.; Mohamed, Z. Evaluation of the Effects of Mitragyna Speciosa Alkaloid Extract on Cytochrome P450 Enzymes Using a High Throughput Assay. *Molecules* **2011**, *16* (9), 7344–7356. https://doi.org/10.3390/molecules16097344.

(15) Chaudhary, K. W.; Clancy, C. E.; Yang, P.; Pierson, J. B.; Goldin, A. L.; Koerner, J. E.; Wisialowski, T. A.; Valentin, J.; Imredy, J. P.; Lagrutta, A.; Authier, S.; Kleiman, R.; Sager, P. T.; Hoffmann, P.; Pugsley, M. K. An Overview of Drug-induced Sodium Channel Blockade and Changes in Cardiac Conduction: Implications for Drug Safety. *Clinical Translational Sci* **2024**, *17* (12), e70098. https://doi.org/10.1111/cts.70098.

(16) Li, Z.; Jin, X.; Wu, T.; Huang, G.; Wu, K.; Lei, J.; Pan, X.; Yan, N. Structural Basis for Pore Blockade of the Human Cardiac Sodium Channel Na_v 1.5 by the Antiarrhythmic Drug Quinidine**. *Angew Chem Int Ed* **2021**, *60* (20), 11474–11480. https://doi.org/10.1002/anie.202102196.

(17) Rouzer, C. A.; Marnett, L. J. Cyclooxygenases: Structural and Functional Insights. *Journal of Lipid Research* **2009**, *50*, S29–S34. https://doi.org/10.1194/jlr.R800042-JLR200.

(18) Rahmawati, S. I.; Indriani, D. W.; Ningsih, F. N.; Hardhiyuna, M.; Firdayani; Ahmadi, P.; Rosyidah, A.; Septiana, E.; Dharmayanti, N. L. P. I.; Bayu, A.; Putra, M. Y. Dual Anti-Inflammatory Activities of COX-2/5-LOX Driven by Kratom Alkaloid Extracts in Lipopolysaccharide-Induced RAW 264.7 Cells. June 25, 2024. https://doi.org/10.21203/rs.3.rs-4628929/v1.

(19) Ikdahl, E.; Kerola, A.; Sollerud, E.; Semb, A. G. Cardiovascular Implications of Non-Steroidal Anti-Inflammatory Drugs: A Comprehensive Review, with Emphasis on Patients with Rheumatoid Arthritis. *Eur Cardiol* **2024**, *19*, e27. https://doi.org/10.15420/ecr.2024.24.

(20) Roma, K.; Mohammed, S.; Sieck, B.; Naik, K.; Wahid, S. Kratom-Induced Acute Liver Injury: A Case Study and the Importance of Herbal Supplement Regulation. *Journal of Hepatology* **2023**, *79* (2), 581–584. https://doi.org/10.1016/j.jhep.2023.04.026.

(21) Patel, P.; Aknouk, M.; Keating, S.; Richard, I.; Kata, P.; Ali, R. Y.; Cheriyath, P. Cheating Death: A Rare Case Presentation of Kratom Toxicity. *Cureus* **2021**. https://doi.org/10.7759/cureus.16582.